Ceramics-Silikáty 66 (2), 167-177 (2022)
www.ceramics-silikaty.cz doi: 10.13168/cs.2022.0011

STRUCTURE AND PROPERTIES OF SILVER-SILICA COMPOSITE PREPARED FROM RICE HUSK SILICA AND SILVER NITRATE

#SIMON SEMBIRING*, AGUS RIYANTO*, IQBAL FIRDAUS*, JUNAIDI*, RUDY SITUMEANG**

*Department of Physics, Faculty of Mathematics and Natural Sciences, University of Lampung, Jl. Prof. Soemantri Brojonegoro, Bandar Lampung, Indonesia 35145
**Department of Chemistry, Faculty of Mathematics and Natural Sciences, University of Lampung, Jl. Prof. Soemantri Brojonegoro, Bandar Lampung, 35145, Indonesia

#E-mail: rudy.tahan@fmipa.unila.ac.id

Submitted January 3, 2022; accepted February 14, 2022

Keywords: Rice husk; Silver; Band gap, Structure; Microstructure; Ag-SiO_2 composite

This research characterises the structure and physical properties of silver/silica (Ag/SiO_2) composites using silver nitrate ($AgNO_3$) and rice husk silica sols as precursors. The Ag/SiO_2 composites were produced with different $AgNO_3$ concentrations (0.3-0.8 M) heated to a temperature of 850 °C. All the composites were fully characterised in the solid state via various techniques; Fourier Transform Infrared Spectroscopy (FTIR), X-ray Diffraction (XRD), Scanning Electron Microcopy/ Energy Dispersive Spectroscopy (SEM/EDS), Thermal Gravimetry Analysis/Differential Thermal Analysis (TGA/DTA) were used to investigate the effects of changes in the sol concentration on the crystalline of Ag/SiO_2 composites. In addition, a Particle Size Analysis (PSA) and a UV-visible technique were used to measure the particle size distribution and band gap energy, respectively. The X-ray diffraction (XRD) showed cristobalite and Ag face-centre-cubic (fcc) structures, indicating the deposition of the Ag particles on the SiO_2 surfaces. The particle size distributions were found to be in a range of 0.01-0.42 µm and 0.49-3.43 µm, followed the band gap energies in a range of 1.97 to 2.17 eV, and 3.63 to 3.57 eV. As a result, the Ag/SiO_2 composite promises to be a great biomedical material degrading high antibacterial properties.

INTRODUCTION

The composite preparation using silver (Ag) in this study, which functions as the active site (dopant), will be distributed to rice husk silica, which acts as a buffer using the sol-gel method. Based on studies from several researchers, they concluded that Ag particles, as the active site, have the ability to degrade and reduce the high antibacterial activity of various bacteria [1-2]. Starting from its wide use such as an antimicrobial, in packaging/ film and food containers, Ag particles have attracted the attention of several researchers in conducting intensive research for their use in various fields as antimicrobial, bacterial and potential agents due to their high surface area to volume ratio, and unique chemical and physical properties [3-6]. However, some disadvantages of Ag particles, such as poor biocompatibility and low dispersion, limit their practical application [7-8]. This limitation has resulted in the continued search for more practical support with a suitable structure.

One of the unique and versatile materials with various applications in the field of ceramic and composite materials is silica (SiO_2), consequently, the need to find a simple and inexpensive source of silica from other materials is an important aspect. In fact, several researchers have explored silica sources as the key materials in the development of nanostructures, which are cheap, clean, and abundant in plant leaves including, bagasse [9-10], rice husks [11], sorghum leaves [12] and lotus leaves [13]. As an example of its uniqueness, silica has the potential as an ingredient in water treatment processes because it has various properties, including its biocompatibility, it is insoluble in water, its chemical stability and high mechanical strength. In this study, the use of rice husk silica as a buffer/matrix in the synthesis of Ag/SiO_2 composites was pioneered because rice husks are extremely abundant, and the silica recovery can be carried out in a simple way, namely alkaline extraction [14-16], with a high silica content, which is 16-20 % of the rice husk weight [17-19].

In addition, the obtained rice husk silica is also known to have an amorphous phase [20-21] and has almost the same ortho silicate structure [22], which is found in transition metal alkoxides and silicon alkoxides, such as tetra ethyl ortho silicates (TEOS) and tetra methyl ortho silicates (TMOS), so that the silica from rice husks has the potential to be used as a substitute for TEOS and TMOS. Based on the physical properties of the silica, such as the large surface area, good heat resistance, high mechanical strength, and inertness, it is shown that the silica can be used as a catalyst [23-24], adsorbent [25], filler [26-27], silica gel [28–29], and composite [30-31]. Associated with the raw material and synthesis method, the silica from rice husks, in the form of sols, has been

obtained with a relatively high silica content and purity [15], which indicates that rice husks have great potential, so that the silica can be utilised directly by the sol-gel method. Regarding the use of rice husk silica, we have conducted several studies in the preparation of materials, including cordierite [32-36], borosilicate [37], mullite [38-39], forsterite [40-41], aluminosilicate [42-43], carbosil [44], and silica-bitumen composites [45-47].

Recognising the important roles of Ag/SiO_2 composites in various industrial fields, the production of Ag/SiO_2 composites has been continuously explored, and, in general, it has been found that the formation of Ag/SiO_2 composites is strongly dependent on the chemical composition, the types of raw material, the presence of impurities, and the preparation methods applied. An important aspect in the Ag/SiO_2 composite is the Ag/SiO_2 preparation method, which basically aims to obtain Ag/SiO_2 containing sufficient amounts and an evenly distributed amount of Ag on the silica buffer surface. The amount of Ag needs to be controlled to get the optimal number of active sites and an even distribution of Ag is needed so that the Ag/SiO_2 composites have consistent performance. Many attempts have been devoted to realising it, including spray [48], deposition [49-50], sol-gel [51-53], impregnation [54], coating [55], and irradiation methods [56].

The impregnation method is known to have weaknesses, especially in the difficulty in obtaining a high dopant homogeneity, while the disadvantage of other methods is the low content of the dopants that can be integrated, despite having high homogeneity. The drawbacks of this other method encourage wider applications of the sol-gel method because it offers various advantages. The sol-gel method is a promising low temperature process which can be controlled to obtain high purity and good compositional homogeneity [57-58], and it is possible to add the dopants simultaneously so that the dopant composition can be adjusted at a certain temperature. In addition, the sol-gel process also produces a stronger dopant-buffer interaction so that the dopant loss during the sintering process can be suppressed. For example, to increase the ability to reduce the antibacterial activity, [59] reported that by immobilising Ag into the silica can reduce the antibacterial concentration of Ag/SiO_2 composites. Several studies related to the utilisation of Ag/SiO_2, include sensors [60], catalysts [61-62], adsorbents [63-64], antibacterial/antimicrobial activities [65], and water purification [66-67].

The characteristics of the synthesised Ag/SiO_2 composite are designed according to their use; some physical properties that need to be designed include the structure formation, thermal resistance, density, porosity, particle size and distribution, and band gap energy. One of the studies that was conducted [68-69] on the effect of the particle size in a range of 1-100 nm showed that the smaller the particle size, the greater its antimicrobial ability. Another study on the formation of Ag/SiO_2 composites [70] showed that Ag was completely trapped in the silica matrix at a sintering temperature of 600 °C, and concluded that the composite had an excellent antibacterial performance. Meanwhile, other researchers [71] showed that Ag/SiO_2 began to form at a sintering temperature of 600 °C and the formation of Ag/SiO_2 was complete at a temperature of 1000 °C, with particle sizes between 20 to 40 nm, which makes it a potential material for an antibacterial activity.

To take advantage of its availability and excellent properties, this present study aimed at evaluating the potential of rice husk silica as an alternative to the commonly used silica for the production of Ag/SiO_2 composites for applications in antibacterial applications and in environments using the sol-gel process. The resulting precursor was then subjected to different Ag concentrations in forming the Ag/SiO_2 composites to determine the phase development and physical properties according to the characteristics for the antibacterial and environmental applications. To gain an insight on several basic characteristics and its potential in antibacterial and environmental functions, the samples were characterised using various techniques including FTIR spectroscopy for a functionality analysis, a XRD technique for a structural investigation, a SEM/EDS technique for a microstructural investigation, a DTA/TGA technique for the thermal properties, a particle size analysis (PSA) technique for the particle size distribution, a UV-vis technique for the band gap value, density and porosity.

EXPERIMENTAL

Materials

To prepare the Ag/SiO_2 composites, analytical grade chemicals were used. The Ag/SiO_2 composites were synthesised through the sol gel route, using rice husk silica collected from local sources and silver nitrate ($AgNO_3$) as the starting materials. The NaOH (5 %), HNO_3 (10 %), and $AgNO_3$ (98 %), absolute ethanol (C_2H_5OH) came from Merck (KGaA, Darmstadt, Germany) and deionised/distilled water was used.

Preparation of silver-silica (Ag/SiO_2) composites

The Ag/SiO_2 composites were prepared by the sol gel process employing rice husk silica with different concentrations of 0.3, 0.4, 0.5, 0.6, 0.7 and 0.8 M silver nitrate ($AgNO_3$). The SiO_2 preparation method was prepared according to a previous procedure [33], 50 grams of rice husk was immersed in 500 ml of the 5 % NaOH solution in a beaker glass and heated to boiling for 30 minutes. The solution was cooled to room temperature and allowed to stand for 24 hours, then it was filtered to separate the filtrate which contains the silica sol. The $AgNO_3$ powder was dissolved in 100 ml of distilled

water and stirred for 30 minutes at room temperature to obtain a silver solution with different concentrations of 0.3, 0.4, 0.5, 0.6, 0.7 and 0.8 M. The procedure of Ag/SiO_2 preparation started with pouring of calculated volumes of silica sol into Ag solution and with addition of HNO_3 and ethanol. Then the mixture was stirred continuously for 4 hours at room temperature using a magnetic stirrer until a completely miscible solution was obtained. The resulting viscous sol was poured into petri dishes and was tightly covered, and the dishes were then put in a closed polypropylene container and left for 3 days to form a solid. The solid was then crushed into a powder with a size of 150 mesh sieve, and sintered at a temperature of 850 ºC, then moulded into a cylindrical pellet and pressed with a pressure of 2×10^4 N m^{-2} to produce cylindrical pellets, ready for analysis.

Physical properties

The density and porosity measurement used the Archimedes [72] principle as follows: ρ = Mdρm (1/Ms – – Mi) where, ρ = the sample density (g·cm^{-3}), ρm = the density of the dyeing medium (g·cm^{-3}), Md = the dry mass sample (g), Mi and Ms are the mass of the saturated sample (immersion mass) and the mass of the saturated sample in air (saturation mass), respectively. The percentage of the porosity (% P) was measured using the equation % P = (Ms – Mi)/(Ms – Md) × 100 %. The particle size distribution was analysed by a particle size analyser (PSA). A UV-vis DRS (wavelength 250-800 nm) and DTA/TGA were used to test the band gap energy value and thermal properties, respectively.

Characterisation

The surface properties, including the functional groups, structure and morphology, thermal and band gap, of the $AgSiO_2$ composites were analysed. FTIR was used to investigate the functional groups in a range of 4000-500 cm^{-1}. The sample was prepared by mixing prepared composites with KBr of spectroscopy grade. The phase composition of the samples was carried out using Shimadzu XD-610 X-ray diffractometer with a Cu-target. The diffractograms were recorded employing radiation (λ = 1.5418 Å) produced at 40 kV and 30 mA, with a 0.15° receiving slit. The diffraction data were analysed using JADE software after subtracting the background and stripping the $CuKa_2$ pattern [73]. The morphological characterization was made by a Philips-XL Scanning Electron Microscopy (SEM) on polished and thermally etched samples. The thermal analysis was performed using a DTA Merck Setaram Tag 24 S, under a nitrogen atmosphere with a constant heating ra-te of 3 °·min^{-1}, at a temperature range of 30 to 1000 °C. The UV-vis spectra of the samples were recorded with a UV/ /Vis Spectrometer (Lambda40, Perkin Elmer, Schwerzenbach, Switzerland) at wavelengths ranging from 250 to 800 nm.

RESULTS AND DISCUSSION

Characteristics of the synthesised Ag/SiO_2 composite

To study the phase development of the Ag/SiO_2 composite, the samples subjected to the Ag addition at different concentrations were characterised using FTIR, XRD and SEM. The FTIR spectra in the wave region of 4000-500 cm^{-1} are shown in Figure 1. Figure 1 shows the infrared spectra of the rice husk silica and Ag/SiO_2 composite with the different Molar Ag at a sintering temperature of 850 °C. The infrared spectrum of the rice husk silica (Figure 1) clearly reveals the presence of two high peaks at 1062 and 794 cm^{-1}, followed by other low peaks at 1635 and 3448 cm^{-1}. The two characteristic bands at 1062 and 794 cm^{-1} are attributed to the vibrational stretching of the asymmetric Si–O–Si in the SiO_4 tetrahedron and the symmetric bond vibration of the Si–O (silanol), respectively, as supported in previous studies [74-75]. The disappearance peaks of the O–H bending and stretching vibration modes in the absorption band region at 3448 and 1635 cm^{-1} confirm the elimination of the hydroxyl or organic groups in the densified powders.

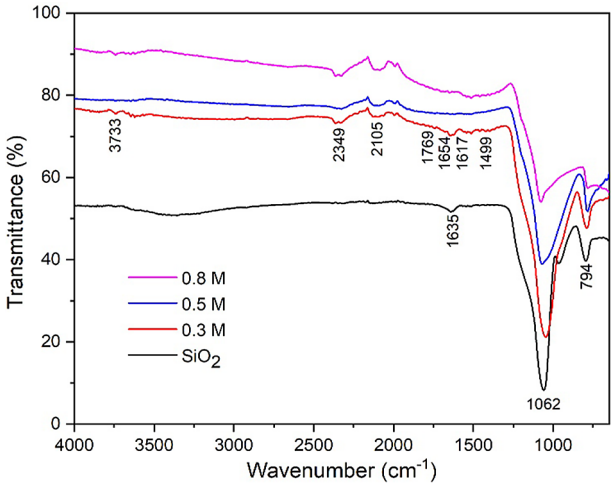

Figure 1. The FTIR spectra of the rice husk silica and Ag/SiO_2 composites with different Molar Ag concentrations at a sintering temperature of 850 °C.

The observed small band is located at 3733 cm^{-1} for the 0.3 M Ag sample (Figure 1), which is commonly attributed to the stretching vibration of the O–H bonds confirming the evaporation of the trapped water and the release of the OH species through the decomposition of the silica and the silver hydroxide molecules into oxides. As a consequence, the band at 794 cm^{-1} is attributed to the ring structure of the SiO_4 tetrahedra. For the 0.3, 0.5 and 0.8 M Ag samples (Figure 1), the most obvious change can be seen in the peak decrease associated with the Si–O–Si stretching vibration and the ring structure of the SiO_4 at band at 1062 and 794 cm^{-1} with an increasing

Ag concentration, confirming the interaction between the silver and silica. The decrease in these bands is caused by the vibrations of the SiO tetrahedral structure and the change in intensity indicates the disorientation of the silver as a result of the interconnection of the silver and silica particles. This behaviour is related to the cristobalite phase of the silica, which proves that the crystallisation of the silica occurs at 850 °C in the Ag/SiO_2 composites. This observation is completely identical with the XRD data. It is also supported by the reappearance of the asymmetric stretching mode of the Si–O–Si bridge and is perhaps evidence for the binding of the Ag to the oxygen of the siloxane bridge that occurs with the evacuation of the water molecules and the reformation of the siloxane bond. The band at 1499 cm^{-1} is attributed to the NO_3^- ions according to the conducted research [70]. The gradual decrease in the NO_3^- ions upon the further increasing Ag concentration can be due to the strongly occurring pyrolysis process of $AgNO_3$ when sintered at a temperature of 850 °C, releasing NO_2 gas. Low peaks appeared at 1769, 1654 and 1617 cm^{-1}, which can be assigned to the stretching vibration of the C=C group and the C=O stretching of the carboxylic acid according to the reported studies [76-78]. Other observed low bonds located at 2349 and 2105 cm^{-1} may show the characteristic functionality groups of O–H from carboxylic acids and C–H from alkanes.

Samples were then analysed using XRD to understand the reaction process of the silver and the silica. Figure 2 shows the XRD patterns of the rice husk silica and Ag/SiO_2 composites with different Molar Ag concentrations at a sintering temperature of 850 °C. The XRD pattern of the rice husk silica (Figure 2) clearly reveals the most intense peak at 2θ = 21.67° and two small peaks at 31.3° and 36.4° indicating the formation of cristobalite (PDF-39-1425).

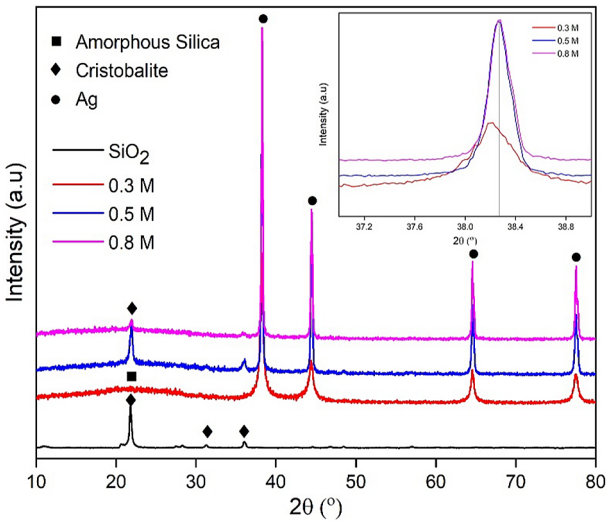

Figure 2. The XRD spectra of the rice husk silica and Ag/SiO_2 composites with different Molar Ag concentrations at a sintering temperature of 850 °C.

After adding 0.3 M Ag (Figure 2), the silica underwent significant changes, i.e., the peak width of 2θ = = 22° in the pattern corresponds to the amorphous silica matrix. The amorphous formation is believed to be due to the silver agglomeration covering the silica particles on the surface, as has also been observed by other studies [79]. In addition to the amorphous silica, five strong Bragg reflections at 2θ = 38.9°, 48.5°, 63.0° 77.5° and 82.6° correspond to the orientation planes of (111), (200), (220), (311) and (222), respectively, which can be indexed according to the facets of the face centre cubic (fcc) crystal structure of the Ag (PDF-4-0862). These confirm the deposition of the Ag particles on the SiO_2 surfaces. For the samples with the 0.5 and 0.8 M Ag concentrations (Figure 2), two phases with a noticeable amount of cristobalite and silver are clearly detected while the amorphous silica is practically undetected. This observation denotes the crystallisation of silica to form cristobalite during the heating process. The most intense peak of Ag in the insert of Figure 2 shows that the crystallinity of the Ag increases with an increasing Ag concentration. It is suggested that the presence of Ag particles favours the crystallisation of the sol-gel derived silica. However, the presence of cristobalite and silver show no reaction between them to form a new phase.

Scanning electron microscopy/energy-dispersive X-ray spectroscopy (SEM/EDX) was used to investigate the nature of the Ag/SiO_2 composites at various Ag concentrations. A typical SEM/EDX analysis is shown in Figure 3a-c and Table 1.

Table 1. Chemical composition of the samples according to the EDX spectra.

Sample (Ag Molar)	O (wt. %)	Si (wt. %)	Ag (wt. %)	Na (wt. %)	Cl (wt. %)
0.3	52.25	27.23	20.52	–	–
0.5	41.08	21.12	37.80	–	–
0.8	44.05	15.15	39.61	1.18	–

As shown in Figure 3a, the surface morphology of the sample was marked by the presence of particles with different grain sizes and distributions, which are indicated by large, medium and fine grains. The large grains are most likely composed of cristobalite, while the medium and fine grains are silver in ellipsoidal shapes. This feature indicates that the silver spherical particles begin to form and spread on the silica matrix. Silver particles can be clearly seen embedded in the SiO_2 matrix (cristobalite) in the samples with higher Ag concentrations (Figure 3b). The particles are well separated from each other and are essentially hemispherical rather than spherical in shape. These results indicate that the cristobalite and silver particles continued to change and, subsequently, the particles began to rearrange, leading to the formation of the Ag/SiO_2 composite. This change is supported by

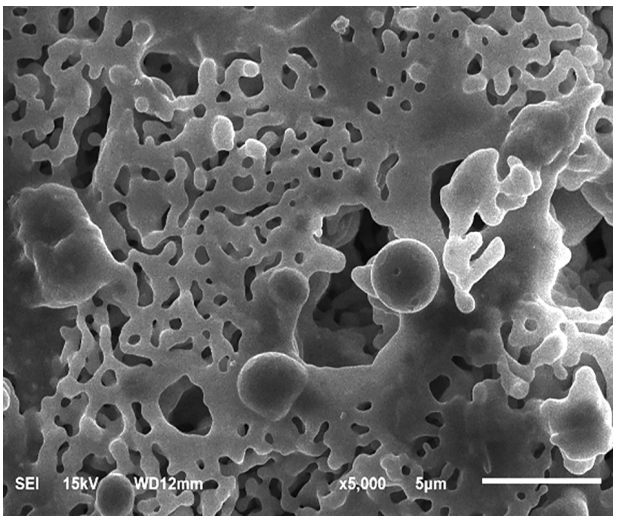

a)

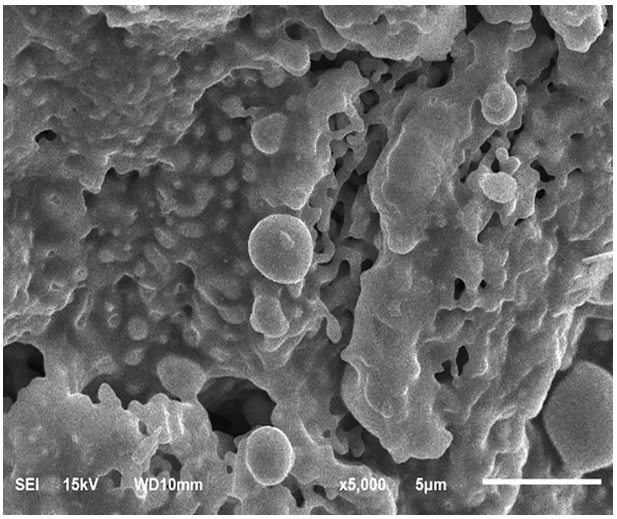

b)

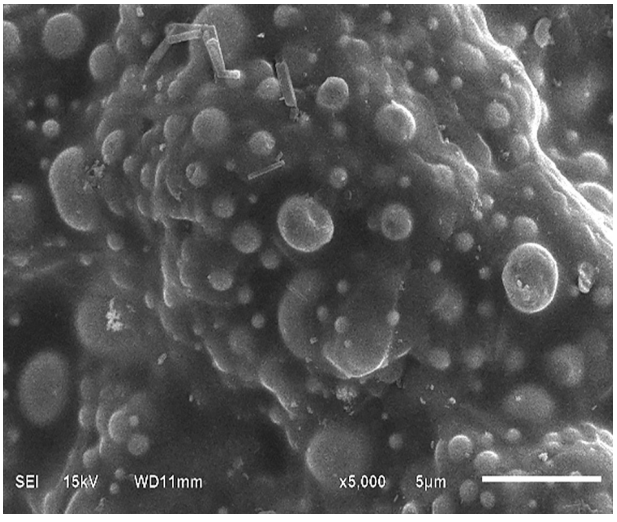

c)

Figure 3. Scanning Electron Micrograph of the Ag/SiO_2 composites with different Ag concentrations at a sintering temperature of 850 °C: a) 0.3 M, b) 0.5 M, and c) 0.8 M (magnification 5 kX).

the result of the XRD analysis for the 0.3 M Ag sample as presented in Figure 2, where amorphous silica was detected. With an increase in the Ag concentration, a significant change occurred. The sample treated at a concentration of 0.8 M Ag (Figure 3c displayed intensified spherical particles that were dispersed almost over the entire surface. Specifically, the microstructure of the sample was found to display particles having a spherical shape with a relatively uniform size on the surface of the silica matrix. This surface characteristics indicate that the silver particles have been converted to a liquid which penetrated the cristobalite phase, thereby promoting the formation of Ag/SiO_2 as the dominant phase, as verified by the XRD results. Also, this result reveals that the Ag particles are well dispersed in the silica matrix or on its surface, and the particle shapes appear almost spherical. The EDX data presented in Table 1 clearly shows the significant effect of the different Ag concentrations on the composition of the samples. As can be seen, the sample with an Ag concentration of 0.3 M, contained a very large amount of Si (27.23 %), and the percentage of this element decreased to 15.15 % in the sample with an Ag concentration of 0.8 M. Meanwhile, the sample with an Ag concentration at 0.3 M contained 20.52 % Ag and increased to 39.61 % with the Ag concentration of 0.8 M. Due to the agglomeration of Ag, the Ag particles interacted with the cristobalite, and the size of the cristobalite group became smaller. The presence of the Ag and SiO_2 (cristobalite) phases in the samples suggest that the cristobalite phase continued to change and allowed the particle arrangement, leading to the expectation of the Ag/SiO_2 composite formation.

Physical characteristics of the synthesised Ag/SiO_2 composite

Figure 4 shows the changes in the density and porosity of the samples as a function of the Ag concentration. As can be observed (Figure 4), the densities of

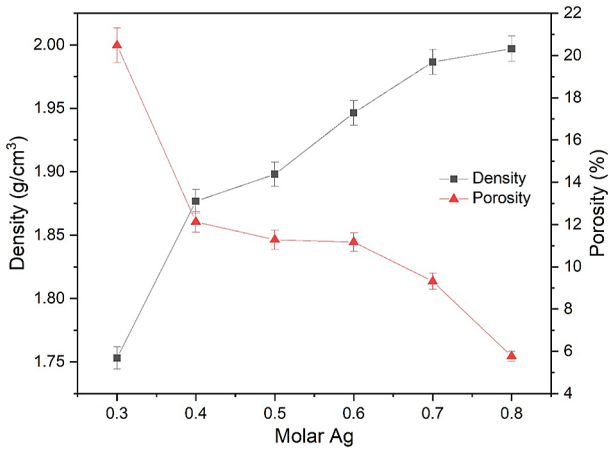

Figure 4. The change in the porosity and density of the Ag/SiO_2 composites with the different Ag concentrations at a sintering temperature of 850 °C.

the samples increase sharply as the Ag concentration increases to 0.4 M and slowly increases when the Ag concentration increases to 0.8 M. Meanwhile, the porosities of the samples decrease sharply as the Ag concentration increases to 0.4 M, and slowly decreases as the Ag concentration increases to 0.8 M. The increase in the density as the Ag concentration increases to 0.4 M is most likely caused by the presence of cristobalite and silver phases as shown in Figure 2.

As shown in Figure 4, the densities of the samples increase from 1.75 to 1.87 g cm^{-3} as the Ag concentration increases from 0.3 to 0.4 M. The densities slowly increased from 1.87 to 1.99 g cm^{-3} as the Ag concentration increased from 0.4 to 0.8 M. The sharp increase in the density with an increasing Ag concentration up to 0.4 M, followed by the slow increase in the density with an increasing Ag concentration from 0.4 to 0.8 M was attributed to the increasing amount of silver phases and the decreasing amount of cristobalite. The change in density was most likely due to the silver and cristobalite reacting to form the Ag/SiO_2 composite, as displayed by the XRD results presented in Figure 2.

The sharp decrease in the porosity with an increasing Ag concentration of up to 0.4 M was attributed to the increasing formation of silver phases, leading to a decreasing porosity. Beyond this concentration, the porosity slowly decreased, probably indicating the domination of the silver, the narrower distances between the particles, and also to the smaller pores in the samples as a result of the higher applied Ag concentration, which is in accordance with the surface morphologies of the samples as seen in the SEM results (Figure 3). Moreover, the porosity was found to decrease as the Ag concentration increased (Figure 4), which is in agreement with an increase in the silver amount (see Table 1). These findings implied that at the temperature used in this study (850 °C), the sample probably has reached the vitrification point and transformed into a glassy state, leading to the suppression of the porosity.

For the further evaluation of the particle size profiles, all the samples were characterised using the PSA technique, and the obtained results are presented in Figure 5. The obtained samples have two main particle distributions in the range of 0.006-0.422 μm and 0.487-3.432 μm as presented in in Figure 5. It should be noted that the particle size distributions of all the samples are inhomogeneous as evidently revealed by the SEM results in Figure 3.

Based on the graph, the average particle size distribution is significantly different, in which the smaller particle sizes and narrower particle size distribution range is very evident. The decrease in the particle size is shown in the 0.3 to 0.5 M Ag sample concentrations. This occurrence may be caused by the reaction between the silver and silica, which dissolved the silver particles in the silica and caused the distribution of the average particle size to become smaller. The data obtained (Figure 5) show that the particle size decreases to a 0.5 M Ag concentration, followed by an increase in the particle size to a 0.8 M Ag concentration. This finding indicates that the silver is easily distributed in the silica particles up to a concentration of 0.5 M, and the silver has difficulty interacting with the silica above an Ag concentration of 0.5 M, resulting in an increasing particle size distribution with an increasing Ag concentration from 0.6 to 0.8 M.

The thermal characteristics of the Ag/SiO_2 composites were observed by TGA/DTA. The TGA thermograms of the samples with the different Ag concentrations are depicted in Figure 6, and the DTA thermograms are presented in Figure 7. The TGA thermogram (Figure 6) shows that all the samples have the same trend in experiencing two major mass loss stages.

In the first stage, at a temperature range from 50 to 200 °C, the small weight loss is attributed to the re-

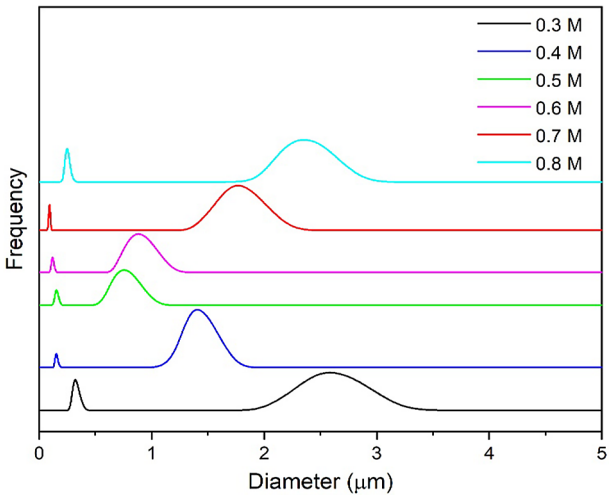

Figure 5. Particle size distribution of the Ag/SiO_2 composites with the different Ag concentration at a sintering temperature of 850 °C.

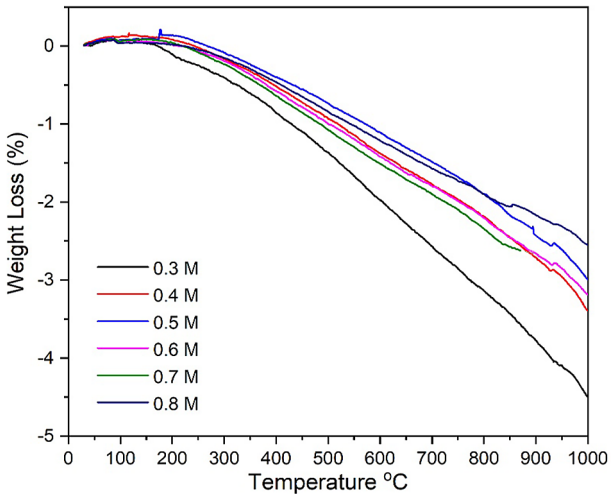

Figure 6. Particle size distribution of the Ag/SiO_2 composites with the different Ag concentration at a sintering temperature of 850 °C.

moval of the physically absorbed water and organic components. The degradation at the second stage occurred in a temperature range from 200 to 850 °C, where the weight loss increased sharply up to 1000 °C. The weight loss of the samples was mainly due to the decomposition of the silver and silicon hydroxides, the saturated and aromatic components, as supported by a previous study [15, 52-53]. One wide exothermic and two small endothermic peaks were found on the DTA curve (Figure 7). The wide exothermic peak located in the range of 50-850 °C indicates the burning of the organic residue, the decomposition and the sample's dryness with compaction above 850 °C.

Table 2. Summary of the TGA properties results for all the samples.

Sample (Ag Molar)	Weight loss (%)		Residue at 1000 °C (%)
	50-200 °C	200-850 °C	
0.3	-0.11	-4.49	95.40
0.4	-0.08	-3.39	96.53
0.5	-0.13	-2.99	96.88
0.6	-0.02	-3.19	96.79
0.7	-0.03	-2.38	97.59
0.8	-0.01	-2.55	97.44

The DTA thermograms of all the samples (Figure 7) show the existence of two small endothermic peaks located at around 850 and 950 °C, respectively. Both endothermic peaks at 850 and 950 °C, were due to the crystallisation of the silica with the presence of cristobalite and silver, as supported by the XRD results presented in Figure 2. On the other hand, for the Ag/SiO_2 composites, no significant reduction in the mass is observed from about 50-1000 °C, indicating the weight loss reduction is in a range of 2.5-4.5 %. This

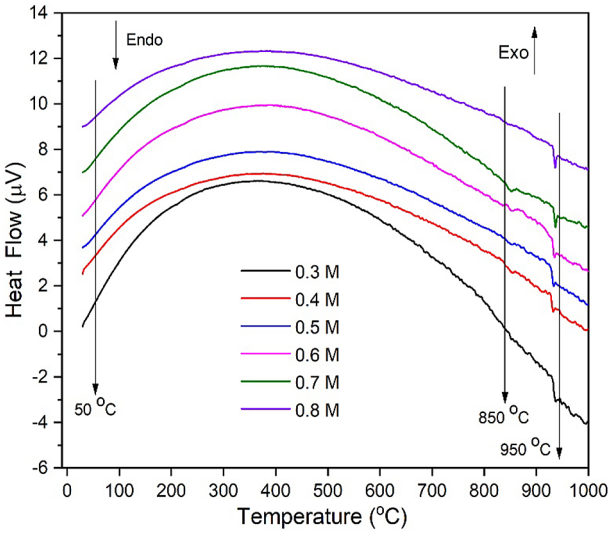

Figure 7. The DTA thermograms of the Ag/SiO_2 composites with the different Ag concentrations at a sintering temperature of 850 °C.

weight loss is attributed to the thermal degradation of the oxide functional groups of the hydroxides process. The weight loss of the Ag/SiO_2 particles confirms the successful incorporation of the silver layer onto the silica particles. The obtained results in Figure 6 and Table 2 also reveal that the weight loss for the Ag/SiO_2 composites is decreased by increasing the Ag concentration of the particles.

Figure 8 shows the band gap energy data for each sample, which is calculated using the Kubelka-Munk Equation [80]. From the plotted graph, as shown in Figure 8, each sample has two optical band gap energies, a primary and secondary one. These suggest that the presence of Ag on the SiO_2 matrix lowers the optical band gap of the samples, compared to the silica with a wide band gap found to be greater than 6 eV by several studies [81-82].

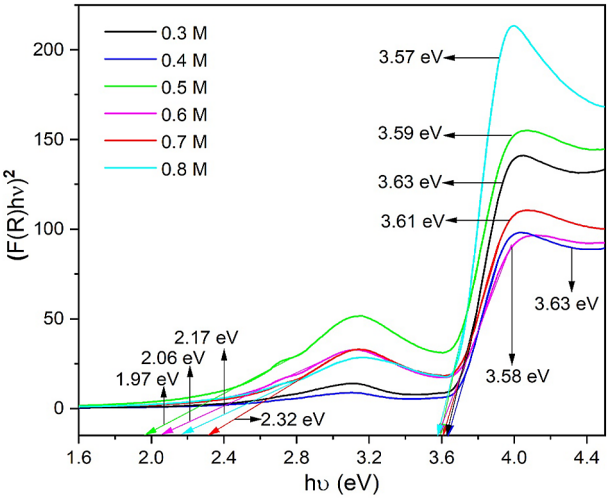

Figure 8. The Kubelka-Munk transferred band gap energy of the Ag/SiO_2 composites with the different Ag concentrations at a sintering temperature of 850 °C. The intersections of the rows with the X-axis represent the values of the band gap energy.

The lower value is probably related to the Ag phase contained within the material while the different Ag phase gives a different value for the band gap energy. In addition, the change in the particle size affects the band gap energy. The presence of the Ag phase in the Ag/SiO_2 composites contributes to decreasing the simultaneous band gap energy value of the composite form. However, after the Ag addition, according to the XRD data, this caused a disturbance in the silica structure and caused the optical band gap value to become lower when compared with the pure silica. Based on the band energy curves in Figure 8, the band energies show two performance areas, namely the pattern of a small increase in the band energy from 1.97 to 2.17 eV, and a small decrease in the band energy from 3.63 to 3.57 eV. The band gap energy value obtained in this study is greater than the energy gap for the pure Ag of 2.5 eV from the results of pre-

vious studies [83]. In another report, Assis, et.al., (2021) [84], produced an Ag/SiO_2 composite with an average band gap energy of approximately 3.26 eV, which has potential advantages for an application as an antibacterial degradation agent.

CONCLUSIONS

A combination of FTIR and XRD analyses with data from DTA/TGA and UV-vis techniques show that the formation of silver crystals results in a significant decrease in the crystallinity of cristobalite and the band gap energy. In addition, with an Ag increasing concentration, this has an effect on the particle size distribution of the Ag/SiO_2 composites and leads to an increase in the density, but does not significantly affect the crystal phase of the Ag/SiO_2 composites. The band gap energies were found to be in the range of 1.97 to 2.17 eV, and 3.63 to 3.57 eV. These powders are potential materials to be used in applications with antibacterial activity.

Acknowledgments

The authors wish to thank the Ministry of Research, Technology, and Higher Education of the Republic of Indonesia for the research funding provided through Superior Research university Grant No: 062/SP2H/LT/DRPM/2022 and DIPA Unila Program for 2022.

REFERENCES

1. Bauer J., Kowal K., Wysocka-Król K., Halina H.P. (2016). Nanosilver and silver doped nanomaterials. in: S.A.M. Tofail, J. Bauer (Eds*.): Electrically Active Materials for Medical Devices*, Imperial College Press, London, 209-224.
2. Martinez-Gutierrez F., Olive P.L., Banuelos A., Orrantia E., Nino N., Sanchez E.M., Ruiz, F., Bach H., Av-Gay Y. (2010): Synthesis, characterization, and evaluation of antimicrobial and cytotoxic effect of silver and titanium nanoparticles. *Nanomedicine*: *Nanotechnology Biology Medicine, 6 (5),* 681-688. doi: 10.1016/j.nano.2010.02.001
3. Garipov I.T., Khaydarov R.R., Gapurova O.U., Rashid A., Khaydarov R.A., Firdaus M.L., Efimova I.L., Evgrafova S.Y. (2019): Silver Nanoparticles as a New Generation of Antimicrobial Prophylaxis. *Journal of Siberian Federal University. Biology, 12(3,* 266-276. doi:10.17516/1997-1389-0301
4. Wang Z., Xia T., Liu S. (2015): Mechanisms of nanosilver-induced toxicological effects: more attention should be paid to its sublethal effects. *Nanoscale*, *7(17)*, 7470–7481. doi: 10.1039/c5nr01133g
5. Khalandi B., Asadi N., Milani M., Davaran S., Abadi A.J., Abasi E., Akbarzadeh A. (2017): A review on potential role of silver nanoparticles and possible mechanisms of their actions on bacteria. *Drug Research***,** *67(2)*, 70-76. doi: 10.1055/s-0042-113383
6. Phu D.V., Lang V.T.K., Lan N.T.K., Duy N.N., Chau N.D., Du B.D., Cam, B.D., Hien, N.Q. (2010): Synthesis and antimicrobial effects of colloidal silver nanoparticles in chitosan by -irradiation. *Journal of Experimental Nanoscience, 5*, 169-179. doi: 10.1080/17458080903383324
7. Xue B., Chen P., Hong Q., Lin J.K., Tan L. (2001): Growth of Pd, Pt, Ag and Au nanoparticles on carbon nanotubes. *Journal of Materials Chemistry, 11*, 2378-2381. doi: 10.1039/b100618p
8. Dong R.X., Chou C.C., Lin J.J. (2009): Synthesis of Immobilized Silver Nanoparticles on Ionic Silicate Clay and Observed Low-Temperature Melting. *Journal of Materials Chemistry, 15*, 2184–2188. doi:10.1039/B818677D
9. Mohd N.K., Wee N.N.A.N., Azmi A.A. (2017): Green synthesis of silica nanoparticles using sugarcane bagasse. *AIP Conference Proceedings, 1885(1),* 020123. doi: 10.1063/1.5002317
10. San N.O., Kurşungöz C., Tümtaş Y., Yaşa Ö., Ortac B., Tekinay T. (2014): Novel one-step synthesis of silica nanoparticles from sugar beet bagasse by laser ablation and their effects on the growth of freshwater algae culture. *Particuology, 17,* 29-35. doi: 10.1016/j.partic.2013.11.003
11. Ghorbani F., Sanati A.M., Maleki M. (2015): Production of silica nanoparticles from rice husk as agricultural waste by environmental friendly technique. *Environmental Studies of Persian Gulf, 2(1)*, 56-65.
12. Qadri S.B., Gorzkowski E.P., Imam M.A., Fliflet A., Goswami R., Kim H., Caldwell J.D., Klemm F., Rath B.B. (2013): Production of nanoscale particles and nanorods of SiC from sorghum leaves, *Industrial Crops and Products. 51*, 158-162. doi: 10.1016/j.indcrop.2013.09.004
13. Landage S.M., Kulkarni S.G., Ubarhande D.P. (2012): Synthesis and application of silica Nano particles on cotton to impart super hydrophobicity. *International Journal of Engineering Research and Technology, 1(5)*, 1-7.
14. Rafieel E., Shahebrahimi S., Feyzil M., Shaterzadeh M. (2012): Optimization of synthesis and characterization of nanosilica produced from rice husk (a common waste material). *International Nano Letters, 2(1)*, 1-8. doi: 10.1186/2228-5326-2-29
15. Ugheoke B.I., Mamat O.A. (2012): A Novel method for high volume production of nano silica from rice husk: process development and product characteristics. *International Material Enggineering Innovation, 3(2)*, 139-155. doi: 10.1504/IJMATEI.2012.046898
16. Tuan L.N.A., Dung L.T.K., Ha L.D.T., Hien N.Q., Phu D.V., Du B.D. (2017): Preparation and characterization of nanosilica from rice husk ash by chemical treatment combined with calcination. *Vietnam Journal of Chemistry, 55*, 446-455. doi: 10.15625/2525-2321.2017-00490
17. Carmona V.B., Oliveira R.M., Silva W.T.L., Mattoso L.H.C., Marconcini J.M. (2013): Nanosilica from rice husk: extraction and characterization. *Industry Crops and Production, 43*, 291-296. doi: 10.1016/j.indcrop.2012.06.050
18. Kumar S., Sangwan P., Dhankhar M.V.R., Bidra S. (2013): Utilization of rice husk and their ash: a review. *Journal of Chemical and Environmental Sciences, 1*, 126-129.
19. Azat S., Korobeinyk A.V., Moustakas K., Inglezakis V.J. (2019): Sustainable production of pure silica from rice husk waste in Kazakhstan. *Journal of Cleaner Production., 217*, 352-359. doi: 10.1016/j.jclepro.2019.01.142

20. Khopthong W., Cherdhirunkorn B. (2020): Production of silica-based ceramics sintered under nitrogen atmosphere from rice husk and sugarcane bagasse ash. *Journal of Metals, Materials and Minerals, 30 (2)*; 76-82. doi: 10.14456/jmmm.2020.23
21. Simanjuntak W., Sembiring S., Pandiangan K.D., Syani F., Situmeang R. (2016): The use of liquid smoke as a substitute for nitric acid of amorphous silica from rice husk through sol-gel route. *Oriental Journal of Chemistry, 32 (4),* 2079-2085. Doi: 10.13005/ojc/32043
22. Mehta A., Ugwekar R.P., (2015): Extraction of silica and other related products from rice husk. *International Enggineering Research and Application, 5(8)*, 43-48.
23. Chen G.Y., Shan R., Shi J.F., Yan B.B. (2015): Transesterification of palm oil to biodiesel using rice husk ash-based catalysts. *Fuel Process Technology, 133*, 8-13. doi: 10.1016/j.fuproc.2015.01.005
24. Adam F., Appaturi J.N., Iqbal A. (2012): The utilization of rice husk silica as a catalyst: review and recent progress. *Catalysis Today,190(1)*, 2-14. doi: 10.1016/j.cattod.2012.04.056
25. Bakar R.A., Yahya R., Gan S.N. (2016): Production of high purity amorphous silica from rice husk. *Procedia Chemistry, 19*, 189-195. doi: 10.1016/j.proche.2016.03.092
26. Dina A.F., Zaleha S.S., Najmi B.N., Azowa I.N. (2014): The influence of alkaline treatment on mechanical properties and morphology of rice husk fiber reinforced polylactic acid. *Advanced Materials Research, 911*, 13-17. doi: 10.4028/www.scientific.net/AMR.911.13
27. Sareeladdanon S., Potiyaraj P. (2014): Mechanical properties of PLA/LLDPE films reinforced with silica from rice husk. *Advanced Materials Research, 1025-1026*, 221-226. Doi: 10.4028/www.scientific.net/AMR.1025-1026.221
28. Tadjarodi A., Haghverdi M., Mohammadi V. (2012): Preparation and characterization of nano-porous silica aerogel from rice husk ash by drying at atmospheric pressure. *Materials Research Bulletin, 47(9)*, 2584-2589. doi: 10.1016/j.materresbull.2012.04.143
29. Feng Q., Chen K., Ma D. (2018): Synthesis of high specific surface area silica aerogel from rice husk ash via ambient pressure drying. *Colloids and Surfaces, A539*, 399-406. Doi: 10.1016/j.colsurfa.2017.12.025
30. Cui J., Cheng F., Lin J., Yang K., Jiang Z., Wen (2017): High surface area C/SiO_2 composite from rice husk as a high-performance anode for lithium-ion batteries. *Powder Technology, 3111*, 1-8. doi: 10.1016/j.powtec.2017.01.083
31. Ju Y., Tang J.A., Zhu K. (2016): SiOx/C composite from rice husk as an anode material for lithium-ion batteries. *Electrochimica Acta, 191*, 411-416 doi:10.1016/j.electacta.2016.01.095
32. Simanjuntak W., Sembiring S. (2011): The use of the Rietveld method to study the phase composition of cordierite ($Mg_2Al_4Si_5O_{18}$) ceramics prepared from rice husk silica. *J. Makara Seri Sains, 15(1)*, 97-100.
33. Sembiring S., Simanjuntak W., Situmeang R., Riyanto A., Sebayang K. (2016): Preparation of refractory cordierite using amorphous rice husk silica for thermal insulation purposes. *Ceramics International, 42*, 8431-8437. doi: 10.1016/j.ceramint.2016.02.062
34. Sembiring S., Simanjuntak W., Situmeang R., Karo-Karo, P. (2017): Effect of alumina addition on refractory properties of cordierite prepared from amorphous rice husk silica. *Journal of Asian Ceramics, 5(2)*, 186-192. doi: 10.1016/j.jascer.2017.04.005
35. Sembiring S., Simanjuntak W., Situmeang R., Riyanto A., Junaidi (2018): Structural and Physical Properties of Refractory Cordierite Precursors Prepared from Rice Husk Silica with Different MgO Addition. *Ceramics-Silikáty 62(2)*, 163-172. doi: 10.13168/cs.2018.0008
36. Sembiring S., Simanjuntak W., Situmeang R. (2019): Structure and Microstructure Properties of a Refractory Cordierite Prepared from Amorphous Rice Husk Silica Resulting from Periclace Introduction. *Journal of Chemical Technology and Metallurgy, 54(4*), 721-726.
37. Sembiring S. (2011): Synthesis and characterisation of rice husk silica-based borosilicate (B_2SiO_5) ceramic by sol gel routes. *Indonesian Journal of Chemistry, 11(1)*, 85-89. doi: 10.22146/ijc.21425
38. Sembiring S., Simanjuntak W. (2012): X-ray diffraction phase analyses of mullite derived from rice husk silica. *Jurnal Makara Seri Sains, 16(2)*, 77-82.
39. Sembiring S., Simanjuntak W., Manurung P., Asmi D., Low I.M. (2014): Synthesis and characterisation of gel-derived mullite precursors from rice husk silica. *Ceramics International, 40(5)*, 7067-7072. doi: 10.1016/j.ceramint.2013.12.038
40. Sembiring S., Riyanto A., Simanjuntak W., Situmeang R. (2017): Effect of MgO–SiO_2 ratio on the forsterite (Mg_2SiO_4) precursors characteristics derived from amorphous rice husk silica. *Journal of Oriental Chemistry, 33*, 186-192. doi: 10.13005/ojc/330427
41. Sembiring S., Riyanto A., Rumiyanti L., Sembiring Z., Situmeang R. (2020): Effect of sintering temperature on the structural and physical properties of forsterite using amorphous rice husk silica as refractory precursors. *Australian Ceramics Society 56*, 433-440. doi: 10.1007/s41779-019-00346-2
42. Simanjuntak W., Sembiring S., Manurung P., Situmeang R., Low I.M. (2013): Characteristics of aluminosilicates prepared from rice husk silica and aluminum metal. *Ceramics International. 39(8)*, 9369-9375. doi: 10.1016/j.ceramint.2013.04.112
43. Riyanto A., Sembiring S., dan Junaidi (2017): Physical characteristics of aluminosilicate geopolymers based on rice husk silica for fast ionic conductor applications. *Reaktor, 17(2)*, 96-103.
44. Simanjuntak W., Sembiring S., Sebayang K. (2012): Effect of pyrolysis temperature on composition and electrical conductivity of carbosil prepared from rice husk. *Indonesian Journal of Chemistry, Universitas Gajah Mada, Jogjakarta, 12(1)*, 119-125. doi: 10.22146/ijc.21350
45. Sembiring S., Situmeang R., Sembiring Z. (2019), Synthesis and characterization of asphalt composite precursors using amorphous rice husk silica. *Ceramica Journal*. *65,* 194-199. doi: 10.1590/0366-69132019653742497
46. Sembiring S., Riyanto A., Situmeang R., Sembiring Z. (2019): Bituminous composite comprising amorphous silica from rice husk. *Ceramics Silikaty*, *63(3)*, 1-9. doi: 10.13168/cs.2019.0021
47. Sembiring S, Riyanto A, Firdaus I., Junaidi, Ningtias E.A. Situmeang R. (2021): Structural characterisation of asphalt-rice husk silica composites. *Ceramics-Silikáty*, 65(3), 215-223. doi: 10.13168/cs.2021.0021
48. Mahltig B., Haufe H., Muschter K., Fischer A., Kim Y.H., Gutmann E., Reibold M., Meyer D.C., Textor T., Kim C.W.,

Kang Y.S. (2010): Silver nanoparticles in SiO_2 microspheres -preparation by spray drying and use as antimicrobial agent. *Acta Chimica Slovenica,* 57(2), 451-457.

49. Duhan S. Devi S., Srivastava M. (2010): Characterization of nanocrystalline Ag/SiO_2 nanocomposites and synthesis by wet chemical method. *Indian J. Pure Applied. Physics, 48*, 271-275.
50. Tuval T., and Gedanken A., (2007): A microwave-assisted polyol method for the deposition of silver nanoparticles on silica spheres. *Nanotechnology, 18(25)*, 255601.
51. Duy P.P., Kim K.H., Cao, V.T., Van Q.V., Thi T.V.T. (2014): Preparation and structural characterization of sol-gel-derived silver silica nanocomposite powders. *International Journal of Materials Science and Applications, 3(35)*, 147-151. doi: 10.11648/j.ijmsa.20140305.13
52. Baheiraei N., Moztarzadeh F., Hedayati M. (2012): Preparation and antibacterial activity of Ag/SiO_2 thin film on glazed ceramic tiles by sol–gel method. *Ceramics International, 38(4),* 2921-2925. doi: 10.1016/j.ceramint.2011.11.068
53. Surender D., Kishoreb N., Aghamkarc P., Sunita D. (2010): Preparation and characterization of sol–gel derived silver-silica nanocomposite. *Journal of Alloys and Compounds, 57,* 101-104. Doi: 10.1016/j.jallcom.2010.07.107
54. Kobayashi Y., Salgueiriño-Maceira V., Liz-Marzán L.M. (2001): Deposition of Silver Nanoparticles on Silica Spheres by Pretreatment Steps in Electroless Plating, *Chemistry Material, 13(5),* 1630-1633. doi: 10.1021/cm001240g
55. Yin Y., Lu, Y., Sun Y., Xia Y.,(2002): Silver Nanowires Can Be Directly Coated with Amorphous Silica to Generate Well-Controlled Coaxial Nanocables of Silver/Silica. *Nano Letters 2(4),* 427-430. doi: 10.1021/nl025508+
56. Nguyen T.K.L., Nguyen T.A.T., Dang V.P., Nguyen N.D., Le A.Q., Nguyen Q.H.,(2013): Synthesis of silver nanoparticles deposited on silica by irradiation and preparation of PE/Ag nano compound masterbatches. *Advances in Natural Sciences: Nanoscience and Nanotechnology, 4,* 1-4. doi: 10.1088/2043-6262/4/4/045004
57. Cao Y., Dai W.L., Deng J.F. (2001): The synthesis, characterization and application of Ag–SiO_2–Al_2O_3 sol-gel composites. *Material Letters*, *50(1),* 12-17. doi: 10.1016/s0167-577x(00)00404-3
58. Pal B.N., Kundu T.K., Banerje S., Charkravorty D. (2003): Humidity sensing by nanocomposites of silver in silicate glass ceramics. *Journal of Applied Physics 93,* 4201. doi: 10.1063/1.1559427
59. Wysocka-Król K., Olsztynska-Janus S., Plesch G., Plecenik A., Podbielska H., Bauer J. (2018): Nano-silver modified silica particles in antibacterial photodynamic therapy. *Applied Surface Science 461,* 260–268. doi: 10.1016/j.apsusc.2018.05.014
60. Ren-Der J., Kuo-Chuang C., Tsung-Han C., Chun-Hua C., Dean-Mo L. (2010): Functionalized Silica Nanoparticles by Nanometallic Ag Decoration for Optical Sensing of Organic Molecule. *Journal of Physics Chemistry C, 114(37),* 15633-15639. doi: 10.1021/jp106185m
61. Zhong-Jie J., Chun-Yan L., Lu-Wei S., Sun (2005): Catalytic Properties of Silver Nanoparticles Supported on Silica Spheres. *The Journal of Physical Chemistry B 109(5),* 1730-1735. doi: 10.1021/jp046032g
62. Kang H., Zhu Y., Yang X., Jing Y., Lengalova A., Li, C. (2010): A novel catalyst based on electrospun silver-doped silica fibers with ribbon morphology., *Journal of Colloid Interface Science 341(2),* 300-310. doi: 10.1016/j.jcis.2009.09.050
63. Das S.K., Khan Md.M.R., Parandhaman T., Laffir F., Guha A.K., Sekaran G., Mandal A.B. (2013): Nano-silica fabricated with silver nanoparticles: antifouling adsorbent for efficient dye removal, effective water disinfection and biofouling control. *Nanoscale, 5(12),* 5549-5560. doi: 10.1039/C3NR00856H
64. Katok K.V., Whitby R.L.D., Fayon F., Bonnamy S., Mikhalovsky S.V., Cundy A.B. (2013): Synthesis and application of hydride silica composites for rapid and facile removal of aqueous mercury. *Chemistry Physics, 14(18),* 4126-4133. http://hdl.handle.net/11455/89436
65. Mosselhy D.A., Granbohm H., Ulla Hynönen U., Ge Y., Palva A Nordström K., Simo-Pekka H. (2017): Nanosilver–Silica Composite: Prolonged Antibacterial Effects and Bacterial Interaction Mechanisms for Wound Dressings. *Nanomaterial, 7(9), (261),* 1-19. doi: 10.3390/nano7090261
66. Ganzagh M.A.A., Yousefpour M., Taherian Z. (2016): The removal of mercury (II) from water by Ag supported on nano mesoporous silica. *Journal Chemistry Biology, 9(4),* 127-142. doi: 10.1007/s12154-016-0157-5
67. Ghosh S., and Vandana V. (2017): Nano-structured mesoporous silver/silica composite: Synthesis, characterization and targeted application towards water purification. *Material Research Bulletin, 88,* 291-300. doi: 10.1016/j.materresbull.2016.12.044
68. Phrabhu S., Poulose E.K. (2012): Silver nanoparticles: mechanism of antimicrobial action, synthesis, medical applications, and toxicity effects. *International Nano Letters,* 2(32), 1-10. doi: 10.1186/2228-5326-2-32
69. Maestre-López M.I., Payà-Nohales J.F., Cuesta-Garrote N., Arán-Ais F., Martínez-Sánchez M.A., Orgilés-Barceló C., Marcelo Bertazzo M. (2015): Antimicrobial Effect of Coated Leather Based on Silver Nanoparticles and Nanocomposites: Synthesis, Characterisation and Microbiological Evaluation. *Journal of Biotechnology & Biomaterials, 5(1),* 1-10. doi: 10.4172/2155-952X.1000171
70. Jeon H.J., Yi S.C., Oh S.G. (2003): Preparation and Antibacterial Effects of Ag-SiO_2 Thin Films by Sol-Gel Method. *Biomaterials, 24,* 4921-4928. doi: 10.1016/S0142-9612(03)00415-0
71. Pham D.P., Huynh K.K., Tran C.V., Vu V.Q., Tran T.T.V. (2014): Preparation and structural characterization of sol-gel-derived silver silica nanocomposite powders. *International Journal of Materials Science and Applications, 3(5),* 147-151.
72. Australian Standard, Refractories and Refractory Material Physical Test Methods (1989): The Determination of Density, Porosity and Water Adsorption, Australian Standard *(1-4),* 1774.
73. JADE Program XRD Pattern Processing PC, Material Data Inc (MDI), Livermore, CA, 1997.
74. Nagai N., Hashimoto H. (2001): FTIR-ATR study of depth profile of SiO_2 ultra-thin films. *Applied Surface Science, 172 (3-4),* 307-311. doi: 10.1016/s0169-4332(00)00867-9
75. Sankar S., Sharma S.K., Kaur N., Lee B., Kim D.Y., Lee S., Jung H. (2016): Biogenerated silica nanoparticles synthesized from sticky, red, and brown rice husk ashes by chemical method. *Ceramic International, 42,* 4875-4885. doi: 10.1016/j.ceramint.2015.11.172
76. Ahsani M., Sabouri R., Ulbricht M., Hazrati H., Jafarizad A., Yegani R. (2021): Preparation and characterization of hydrophilic and antibacterial silver decorated silica-grafted-poly (vinylpyrrolidone) (Ag–SiO_2–PVP) nanoparticles for

polymeric nanocomposites. *Journal of Applied Polymer Science*, *e50977,* 1-12. doi: 10.1002/app.50977

77. Javadi M., Jafarzadeh Y., Yegani R., Kazemi S. (2018): PVDF membranes embedded with PVP Functionalized nanodiamond for pharmaceutical wastewater treatment. *Chemical Engineering Research Design, 140,* 241-250. doi:10.1016/j.cherd.2018.10.029
78. Manikandan V., Velmurugan P., Jung-Hee P., Woo-Suk C., Yool-Jin P., Jayanthi P., Cho M., Byung-Taek O. (2017): Green synthesis of silver oxide nanoparticles and its antibacterial activity against dental pathogens. *Biotechnology, 7(72),* 1-9. doi: 10.1007/s13205-017-0670-4
79. Prakash P., Gnanaprakasam P., Emmanuel R., Arokiyaraj S., Saravanan M. (2013): Green synthesis of silver nanoparticles from leaf extract of Mimusops elengi, Linn. for enhanced antibacterial activity against multi drug resistant clinical isolates. *Colloid and Surface B, Biointerfaces. 108,* 255-259. doi: 10.1016/j.colsurfb.2013.03.017
80. Escobedo Morales A., Sanchez Mora E., Pal U. (2007): Use of diffuse reflectance spectroscopy for optical characterization of un-supported nanostructures. *Revista Mexicana de Fisica, S 53 (5),* 18-22.
81. Nithianandam V.J., Schnatterly S.E. (1988): Soft-x-ray emission and inelastic electron-scattering study of the electronic excitations in amorphous and crystalline silicon dioxide. *Physical Review, B, 38,* 5547. doi: 10.1103/PhysRevB.38.5547
82. Hassan A.F., Abdelghny A.M., Elhadidy H., Youssef A.M. (2014): Synthesis and characterization of high surface area nanosilica from rice husk ash by surfactant-free sol–gel method. *Sol-Gel Science and Technology, 69(3),* 465-472. doi: 10.1007/s10971-013-3245-9
83. Aziz A., Khalid M., Saeed akhtar M., Nadeem M., Gilani Z.A., Ul huda khan asghar H.M.N., Rehman Ullah Z., Saleem M. (2018): Structural, morphological and optical investigations of silver nanoparticles synthesized by sol-gel autocombustion method. *Digest Journal of Nanomaterial and Biostructure, 13(3),* 679-683.
84. Assis M., Simoes L.G.P., Tremiliosi G.C., Coelho D., Minozzi D.T., Santos R.I., Vilela D.C.B., do Santos J.R., Ribeiro L.K., Rosa I.L.V., Mascaro L.H., Andrés J., Longo E. (2021): SiO_2-Ag composite as a highly virucidal material: A roadmap that rapidly eliminates SARS-CoV-2. *Nano material, 11(638),* 1-19. doi: 10.3390/nano11030638